AMERICAN SOCIETY FOR MICROBIOLOGY | Journal of Virology

| Virology | Full-Length Text

Rational attenuation of canine distemper virus (CDV) to develop a morbillivirus animal model that mimics measles in humans

Katharina S. Schmitz,[1] Linda J. Rennick,[2] Natasha L. Tilston-Lunel,[2] Anouskha D. Comvalius,[1] Brigitta M. Laksono,[1] Daryl Geers,[1] Peter van Run,[1] Rory D. de Vries,[1] Rik L. de Swart,[1] W. Paul Duprex[2]

AUTHOR AFFILIATIONS See affiliation list on p. 11.

ABSTRACT Morbilliviruses are members of the family Paramyxoviridae and are known for their ability to cause systemic disease in a variety of mammalian hosts. The prototypic morbillivirus, measles virus (MeV), infects humans and still causes morbidity and mortality in unvaccinated children and young adults. Experimental infection studies in non-human primates have contributed to the understanding of measles pathogenesis. However, ethical restrictions call for the development of new animal models. Canine distemper virus (CDV) infects a wide range of animals, including ferrets, and its pathogenesis shares many features with measles. However, wild-type CDV infection is almost always lethal, while MeV infection is usually self-limiting. Here, we made five recombinant CDVs, predicted to be attenuated, and compared their pathogenesis to the non-attenuated recombinant CDV in a ferret model. Three viruses were insufficiently attenuated based on clinical signs, fatality, and systemic infection, while one virus was too attenuated. The last candidate virus caused a self-limiting infection associated with transient viremia and viral dissemination to all lymphoid tissues, was shed transiently from the upper respiratory tract, and did not result in acute neurological signs. Additionally, an in-depth phenotyping of the infected white blood cells showed lower infection percentages in all lymphocyte subsets when compared to the non-attenuated CDV. In conclusion, infection models using this candidate virus mimic measles and can be used to study pathogenesis-related questions and to test interventions for morbilliviruses in a natural host species.

IMPORTANCE Morbilliviruses are transmitted via the respiratory route but cause systemic disease. The viruses use two cellular receptors to infect myeloid, lymphoid, and epithelial cells. Measles virus (MeV) remains an important cause of morbidity and mortality in humans, requiring animal models to study pathogenesis or intervention strategies. Experimental MeV infections in non-human primates are restricted by ethical and practical constraints, and animal morbillivirus infections in natural host species have been considered as alternatives. Inoculation of ferrets with wild-type canine distemper virus (CDV) has been used for this purpose, but in most cases, the virus overwhelms the immune system and causes highly lethal disease. Introduction of an additional transcription unit and an additional attenuating point mutation in the polymerase yielded a candidate virus that caused self-limiting disease with transient viremia and virus shedding. This rationally attenuated CDV strain can be used for experimental morbillivirus infections in ferrets that reflect measles in humans.

KEYWORDS measles, canine distemper, ferret, model, attenuation

Measles virus (MeV) is an airborne morbillivirus in the family Paramyxoviridae (1) and causes an acute disease characterized by fever and rash. The introduction of live-attenuated measles vaccines in the 1960s significantly reduced measles morbidity

Editor Rebecca Ellis Dutch, University of Kentucky College of Medicine, Lexington, Kentucky, USA

Address correspondence to Rik L. de Swart, r.deswart@erasmusmc.nl.

The authors declare no conflict of interest.

See the funding table on p. 11.

Received 27 November 2023
Accepted 5 February 2024
Published 28 February 2024

and is estimated to have averted more than 55 million deaths between 2000 and 2021 globally (2). After a global measles surge from 2017 to 2019, case numbers dropped again in 2020 and 2021 as a result of non-pharmaceutical COVID-19 interventions. However, the pandemic also resulted in reduced measles vaccination coverage, leaving more than 25 million children at risk for measles (2).

Initial MeV infection and replication are largely restricted to cell types that express the cellular entry receptor human signaling lymphocyte activation molecule F1 (hSLAMF1 or CD150). MeV infection is initiated in myeloid cells like dendritic cells (DCs) and alveolar macrophages (3, 4). Systemic dissemination is facilitated by circulating CD150-expressing B- and T-lymphocytes, whose depletion results in transient lymphopenia and immune suppression (5, 6). This causes increased susceptibility to secondary infections, which are responsible for the majority of measles-associated morbidity and mortality. Peripheral blood lymphocyte cell counts are usually restored within 2–3 weeks post-infection, but the immune suppression can last up to 2–3 years after measles (7). The preferential infection and depletion of CD150-expressing memory lymphocytes are the underlying cause of "immune amnesia", a status in which lymphocyte numbers are restored, but the pre-measles immune repertoire is impaired (5, 6, 8–10). Ultimately, infiltration of MeV-infected immune cells into the respiratory submucosa results in infection of epithelial cells via nectin-4, a second cellular receptor that is part of the adherens junctions and, in differentiated epithelial cells, can only be reached from the basolateral side (11–13).

Unraveling the mechanisms underlying measles immune suppression was largely based on studies in experimentally infected macaques; the use of non-human primates (NHPs) in measles research has greatly facilitated our understanding of measles pathogenesis (14). However, NHP studies are becoming ethically and practically more challenging, resulting in a need for new animal models. Most rodents are not susceptible or permissive to wild-type (WT) MeV. Transgenic mice that overexpress the human MeV receptors are used as animal models (15, 16) but poorly recapitulate measles pathogenesis. Alternatively, animal morbilliviruses can be studied in natural hosts as a surrogate model for measles. Canine distemper virus (CDV) infects a broad host range of carnivores and omnivores, including dogs, ferrets, and raccoons (17, 18). CDV infection of ferrets has often been used as a surrogate model (19). CDV replication in ferrets largely resembles the natural course of MeV infection in primates (20). Importantly, while measles is usually not fatal in NHPs, WT CDV infection of ferrets can lead to high case fatality rates. Experimental infection of ferrets with a rationally attenuated CDV could be used as an improved animal model of disease for measles. This model could be used to address open questions such as the impact of measles on acquired immunity by vaccines and viral infections and, hence, inform if re-vaccination with typical childhood vaccines post measles should be recommended. Moreover, this model could also be used to study new strategies for measles prevention or treatment.

Several approaches have been used to attenuate morbilliviruses: (i) Morbillivirus replication is characterized by a transcriptional gradient, leading to more expression of the first encoded gene (nucleoprotein, N) than the gene encoded last (large protein, L) in the viral genome (21). Adding an additional transcription unit (ATU) proximal to N (position 1) attenuated CDV (22). (ii) Deleting the C protein may decrease CDV pathogenicity as this protein, expressed from an alternative open reading frame of the P gene, has been shown to be critical for MeV virulence (23). (iii) The insertion of enhanced green fluorescent protein (EGFP) into L was used to attenuate rinderpest virus (RPV), a morbillivirus closely related to MeV, and a highly pathogenic CDV strain (24, 25). (iv) A single-point mutation in L (H589Y) attenuated CDV in ferrets, resulting in the survival of two-thirds of animals, while all control animals succumbed to the infection (26). (v) Modifications of CDV hemagglutinin (H) rendered it unable to bind CD150 or nectin-4 (receptor-blind viruses) resulting in attenuated phenotypes (27, 28).

We set out to develop a rationally attenuated CDV that could be used for experimental infections of ferrets, resulting in an animal model of disease that mimics measles in

humans. Before embarking on these studies, we defined a number of desired characteristics of the virus to resemble known properties of MeV as observed in humans and NHPs, based on previously published data (6–8, 27, 29–32): (i) CDV should use CD150 and nectin-4, and (ii) the infection should be self-limiting, i.e., non-lethal. CDV should cause (iii) transient lymphopenia, (iv) transient viremia, and should (v) result in spread to lymphoid tissues. Moreover, CDV should (vi) be transiently shed from the upper respiratory tract but (vii) not cause clinical signs that reflect acute central nervous system (CNS) infection.

A recombinant CDV (rCDV) containing an ATU encoding Venus fluorescent protein at position 6 (proximal to L) and based on a full-genome sequence obtained from a naturally infected raccoon in Rhode Island, USA, was recently generated [rCDV^{RI}Venus(6)] (33). We studied the pathogenesis of this recombinant virus in raccoons (18) and ferrets (34). Here, we made five different recombinant CDVs based on this recombinant virus and compared attenuation of these viruses relative to infection with rCDV^{RI}Venus(6) in ferrets. We evaluated clinical signs, case fatality, lymphopenia, viral shedding, viremia, and virus load in lymphoid tissues. Finally, we propose a recombinant CDV attenuated by insertion of an ATU at position 1 and an additional attenuating point mutation in L (H589Y) as a candidate virus to be used in a ferret model to mimic measles pathogenesis.

RESULTS

Clinical signs

Five different rCDVs were made by inserting an ATU at position 1 [rCDV^{RI}Venus(1)] (22), combining insertion of an ATU at position 6 or position 1 with an additional mutation in L [H589Y; rCDV^{RI}Venus(6)-L$_{H589Y}$ and rCDV^{RI}Venus(1)-L$_{H589Y}$] (26), combining insertion of an ATU at position 6 with insertion of EGFP into the polymerase [rCDV^{RI}Venus(6)-L$_{EGFP}$] (24, 25), or combining insertion of an ATU at position 6 with deletion of the C protein [rCDV^{RI}Venus(6)-ΔC] (23) (Fig. 1). All recombinant viruses used the cellular receptors CD150 and nectin-4 (Fig. S1).

Ferrets inoculated with rCDV^{RI}Venus(6) presented with a fever from 3 dpi onward, which peaked at 6 dpi and stayed elevated until they reached their humane endpoints (Fig. 2A). This pattern was similar for animals inoculated with rCDV^{RI}Venus(6)-ΔC and rCDV^{RI}Venus(1). Five out of seven animals inoculated with rCDV^{RI}Venus(6)-L$_{H589Y}$ had a transient fever, while two animals presented with prolonged elevated body temperature until they reached their humane endpoint or the end of the study period was reached. All rCDV^{RI}Venus(1)-L$_{H589Y}$-inoculated ferrets experienced a transient fever peaking on day 6, whereas animals inoculated with rCDV^{RI}Venus(6)-L$_{EGFP}$ did not develop fever at all. Next, we determined the severity score (0–3), an average score of body temperature, body weight, lymphocyte counts, virus isolation from throat swabs, and infection of lymphocytes in blood (viremia) (Fig. 2B; Table S1). As MeV does not productively

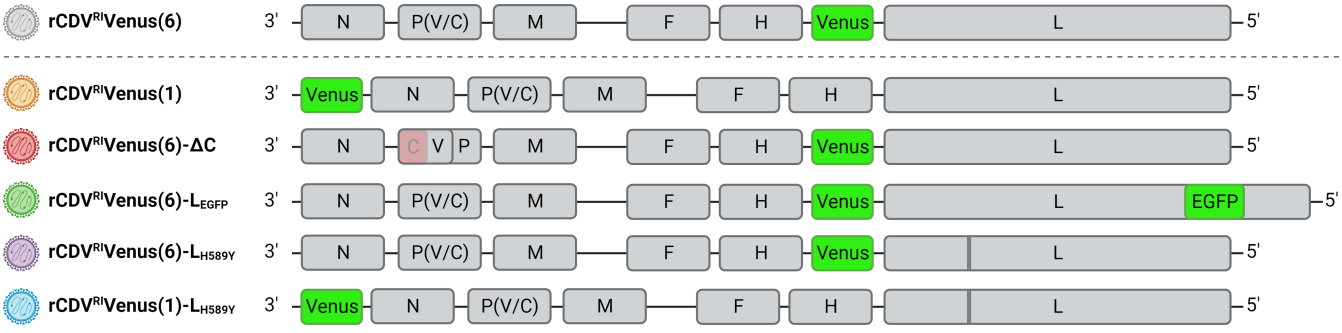

FIG 1 Schematic overview of rCDV constructs. Attempted rational attenuation of rCDV^{RI} by introducing an ATU (Venus) in position 1 (brown), or deleting the C protein (red), introducing EGFP into the L gene (green), or mutating position 589 (vertical line) of the L gene (purple) of rCDV^{RI}Venus(6), or introducing Venus at position 1 and mutating position 589 of the L gene (blue). rCDV^{RI}Venus(6), previously shown to be pathogenic in ferrets and raccoons, is shown in gray for comparison. The colors for the different rCDVs are consistent throughout the manuscript.

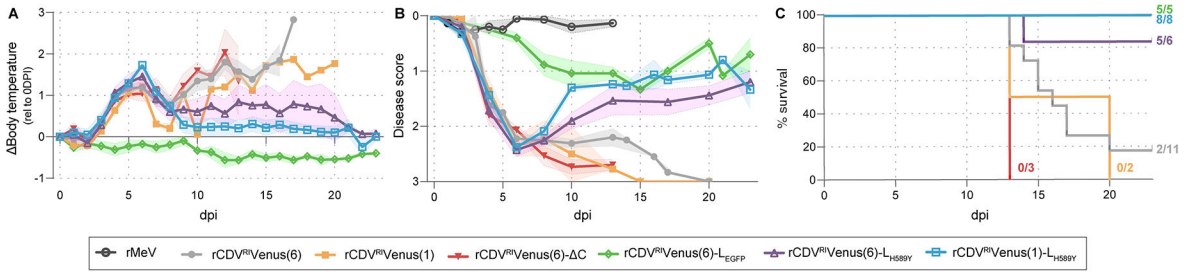

FIG 2 Clinical parameters of ferrets inoculated with different rCDVs. (A) Change in body temperature relative to day 0 for animals inoculated with different rCDVs (in degrees celcius). (B) The severity score, an average score of body temperature, body weight, lymphocyte count, virus isolation from throat swabs, and infection of lymphocytes for all rCDVs. The severity score of MeV-inoculated ferrets is shown as a negative control. Shaded bands depict the standard error of the mean (SEM). (C) Kaplan-Meier curve depicting the percentage survival of animals in each group.

replicate in ferrets and therefore does not cause disease (34), we used MeV-inoculated ferrets, which had a stable severity score of 0, as controls. rCDV^{RI}Venus(6)-L$_{EGFP}$-inoculated ferrets had a peak score of 1. All other animals reached a severity score of >2 by day 6; animals inoculated with rCDV^{RI}Venus(6)-L$_{H589Y}$ and rCDV^{RI}Venus(1)-L$_{H589Y}$ partly recovered, while the severity score for rCDV^{RI}Venus(6)-, rCDV^{RI}Venus(6)-ΔC-, and rCDV^{RI}Venus(1)-inoculated animals did not decrease. Ultimately, the severe phenotype of rCDV^{RI}Venus(6)-ΔC and rCDV^{RI}Venus(1) was confirmed as all animals reached their humane endpoints, while no ferrets succumbed to infection for the rCDV^{RI}Venus(6)-L$_{EGFP}$ variant or the rCDV^{RI}Venus(1)-L$_{H589Y}$ variant (Fig. 2C). One out of six ferrets inoculated with rCDV^{RI}Venus(6)-L$_{H589Y}$ reached its humane endpoints and was euthanized.

CDV shedding

We compared rCDV shedding patterns by obtaining throat, nose, and rectal swabs throughout the study period (Fig. 3). Generally, virus titers in the throat (Fig. 3A) were slightly higher than those obtained from rectal swabs (Fig. 3B). The lowest amount of virus was detected in the nose (Fig. 3C). rCDV^{RI}Venus(6)-L$_{EGFP}$ was shed for the shortest duration and to only low titers (<10^2 TCID$_{50}$/mL). In contrast, rCDV^{RI}Venus(6), rCDV^{RI}Venus(1), and rCDV^{RI}Venus(6)-ΔC were all detected from 4 dpi onward until all animals reached their humane endpoints, and at their peak throat, nose, and rectal swab viral titers for these variants exceeded the titers observed for other rCDV variants. Shedding of both polymerase point mutation viruses was transient; however, shedding for rCDV^{RI}Venus(6)-L$_{H589Y}$ was of higher magnitude and longer duration when compared to rCDV^{RI}Venus(1)-L$_{H589Y}$.

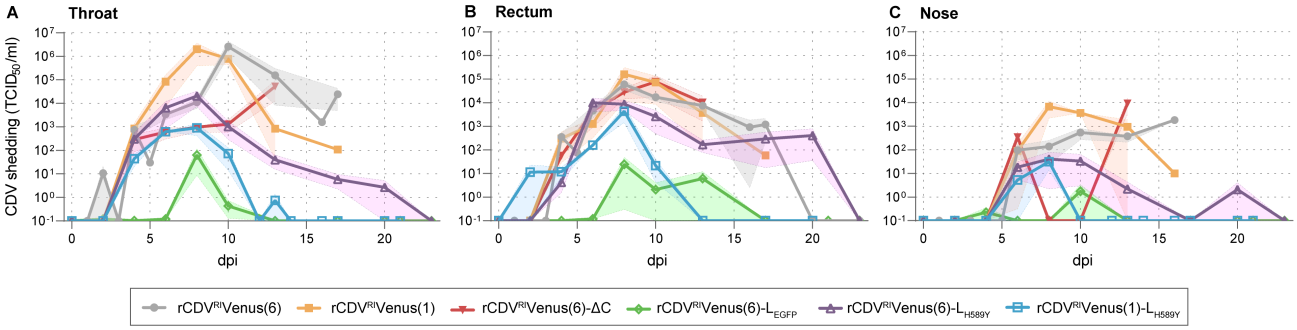

FIG 3 Shedding of rCDVs. Infectious rCDVs were isolated from (A) throat, (B) rectum, and (C) nose swabs on VDS cells. Titers were determined by endpoint titration and are expressed as TCID$_{50}$/mL. Shaded bands depict the SEM.

CDV viremia and lymphopenia

Next, we evaluated the infection of WBC and resulting lymphopenia in animals inoculated with the rCDVs (Fig. 4). To this end, we titrated WBC isolated from whole blood (Fig. 4A) and determined the infection percentage of lymphocytes by flow cytometry (Fig. 4B). The two variants that previously appeared insufficiently attenuated [rCDV^{RI}Venus(6)-ΔC, rCDV^{RI}Venus(1)], mimicked the pattern observed for rCDV^{RI}Venus(6). Notably, at its peak at 6 dpi, lymphocyte infection percentages of rCDV^{RI}Venus(6)-ΔC- and rCDV^{RI}Venus(1)-inoculated animals exceeded those of the control group with >80% and >60%, respectively (Fig. 4B). Viremia of rCDV^{RI}Venus(6)-L$_{EGFP}$-inoculated animals appeared much later, and less virus could be isolated when compared to all other variants (Fig. 4A), which was also represented by the lower infection percentages (Fig. 4B). Viral titers from WBC and infection percentages of lymphocytes from ferrets inoculated with the polymerase point mutation viruses were similar. Virus was isolated from 2 dpi onward, and infectious virus loads peaked at 6 dpi (Fig. 4A). Peak infection percentages at 6 dpi were between 30% and 40% and declined afterward (Fig. 4B). With the exception of rCDV^{RI}Venus(6)-L$_{EGFP}$-inoculated animals, resulting changes in lymphocyte counts were similar for most animals (Fig. 4C). Lymphocyte counts dropped from 4 dpi onward, were lowest between 5 and 6 dpi, and stayed low for the entire study period. As an exception, lymphopenia of rCDV^{RI}Venus(6)-L$_{EGFP}$-inoculated ferrets was observed relatively late (from 8 dpi onward), and fully recovered by 20 dpi, additionally indicating mild disease in these ferrets as compared to animals inoculated with the other rCDVs.

Based on these findings, we identified rCDV^{RI}Venus(1)-L$_{H589Y}$ for in-depth characterization as a "MeV-like" virus; the other candidate viruses were either insufficiently [rCDV^{RI}Venus(6)-ΔC, rCDV^{RI}Venus(1)] or too attenuated (rCDV^{RI}Venus(6)-L$_{EGFP}$) and did not mimic measles pathogenesis (Fig. S2). Although rCDV^{RI}Venus(6)-L$_{H589Y}$ behaved similarly to rCDV^{RI}Venus(1)-L$_{H589Y}$ in our study, the higher case fatality rate (CFR) with CNS involvement (1/6) (Fig. 2C), the slightly higher overall severity score (Fig. 2B), and the prolonged shedding (Fig. 3) of the rCDV^{RI}Venus(6)-L$_{H589Y}$-inoculated ferrets made us choose rCDV^{RI}Venus(1)-L$_{H589Y}$ as our candidate-attenuated CDV.

Phenotyping of CDV-infected white blood cells

Next, we characterized the phenotype of rCDV^{RI}Venus(1)-L$_{H589Y}$-infected cells and compared this to rCDV^{RI}Venus(6)-infected cells. To this end, we identified WBCs as Th-lymphocytes, Tc-lymphocytes, B-lymphocytes, DCs, monocytes, and granulocytes using forward scatter (FSC), side scatter (SSC), and cell-surface markers (Fig. S3). For all subsets, we gated Venus$^+$ cells to identify the target cells of rCDV^{RI}Venus(1)-L$_{H589Y}$. Similar to what was observed for rCDV^{RI}Venus(6), the majority of infected cells were Th-lymphocytes (Fig. 5A and B). While on average, more than 90% of Th-lymphocytes were infected with rCDV^{RI}Venus(6) at the peak of infection, this was approximately 80%

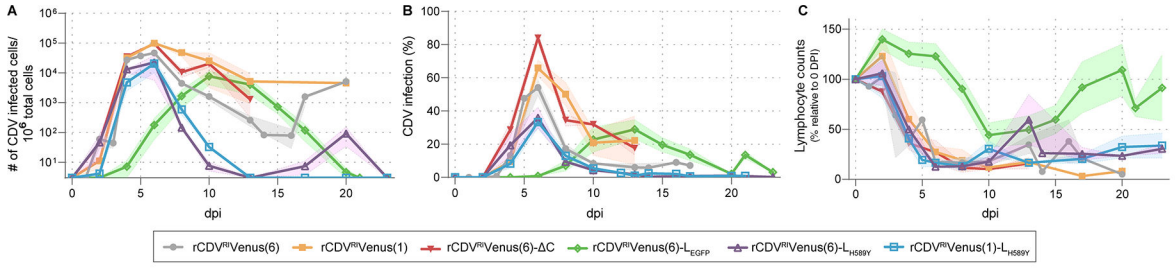

FIG 4 rCDV viremia and lymphopenia. Detection of rCDVs in peripheral blood via (A) virus isolation or (B) flow cytometry. (A) WBCs obtained from rCDV-inoculated ferrets were titrated on VDS cells, and viral loads were expressed as the number of infected cells per 10^6 total cells. (B) Infection percentage of ferret lymphocytes measured by flow cytometry. The percentage of Venus$^+$ cells in the singlet lymphocyte gate was determined. (C) Lymphocyte counts are shown relative to day 0 for animals inoculated with the different rCDVs. Shaded bands depict the SEM.

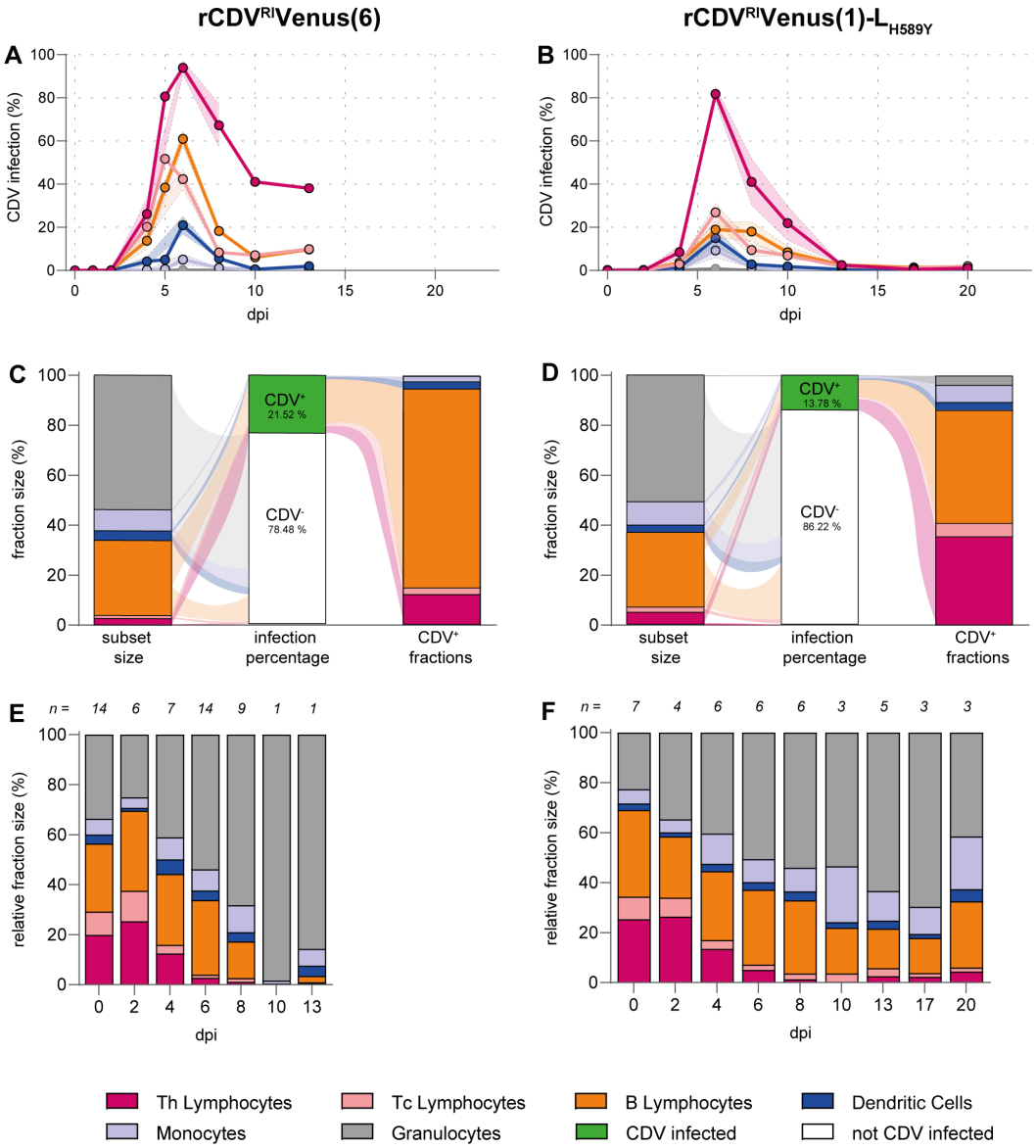

FIG 5 Phenotype of rCDV^{RI}Venus(1)-L$_{H589Y}$-infected WBC in comparison to rCDV^{RI}Venus(6)-infected WBC. (A and B) Infection percentage of different cell types measured by flow cytometry. The percentage of Venus$^+$ cells in the indicated population was determined for (A) rCDV^{RI}Venus(6) and (B) rCDV^{RI}Venus(1)-L$_{H589Y}$. Per time point, all available samples were evaluated. Shaded bands indicate the SEM. (C and D) Phenotyping of rCDV-infected cells on 6 dpi via inverse gating of Venus$^+$ cells within the singlet gate. The relative population sizes are shown as the average population sizes of (C) n = 14 rCDV^{RI}Venus(6)-infected ferrets and (D) n = 6 rCDV^{RI}Venus(1)-L$_{H589Y}$-infected ferrets. (E and F) Subsets of WBC were identified in peripheral blood via flow cytometry at the indicated time points for (E) rCDV^{RI}Venus(6) and (F) rCDV^{RI}Venus(1)-L$_{H589Y}$. The relative population size at each time point is shown as the average population size of all available samples per time point. The gating strategy can be found in Fig. S3.

for rCDV^{RI}Venus(1)-L$_{H589Y}$. Surprisingly, the percentages of infected Tc-lymphocytes and B-lymphocytes were much lower for rCDV^{RI}Venus(1)-L$_{H589Y}$-inoculated animals when compared to rCDV^{RI}Venus(6)-inoculated ferrets (approx. 20% vs 50%–60%, respectively). Percentages of infection of DCs and monocytes were similar in both groups; granulocytes were hardly infected by CDV. Moreover, we compared phenotypes at the peak of infection (6 dpi) for rCDV^{RI}Venus(6) and rCDV^{RI}Venus(1)-L$_{H589Y}$. For rCDV^{RI}Venus(6), the majority of infected cells were B-lymphocytes, while for rCDV^{RI}Venus(1)-L$_{H589Y}$, similar amounts of T- and B-lymphocytes were infected (Fig. 5C and D).

Consequently, in addition to overall lymphopenia observed (Fig. 4C), we also detected a change in the relative fraction of WBC (Fig. 5E and F). At 4 dpi, a relative decrease in Th-

and Tc-lymphocytes was detected for both groups. For rCDV^{RI}Venus(6)-inoculated ferrets, all lymphocyte fractions declined further over time, resulting in no T-lymphocytes at 10 dpi and only limited numbers of B-lymphocytes at 13 dpi (N = 1 for 10 and 13 dpi) (Fig. 5E). Relative lymphocyte fractions also decreased for rCDV^{RI}Venus(1)-L$_{H589Y}$-inoculated ferrets, but at all evaluated time points, a fraction of B-lymphocytes remained (Fig. 5F). At 20 dpi, T-lymphocyte fractions were still low (<10%), but B-lymphocyte, DC, and monocyte fractions recovered, indicating overall rehabilitation of the immune system of rCDV^{RI}Venus(1)-L$_{H589Y}$-inoculated ferrets.

rCDV^{RI}Venus(1)-L$_{H589Y}$ in lymphoid tissues

Last, we compared the spread of rCDV^{RI}Venus(1)-L$_{H589Y}$ to the spread of rCDV^{RI}Venus(6) in lymphoid tissues and lungs over time (Fig. 6). Organs were harvested upon euthanization, and the data presented depict individual animals. At the early time points (4 and 6 dpi), infection percentages of mandibular, tracheobronchial, axillar, inguinal, and mesenteric lymph nodes as well as broncho-alveolar lavage cells, thymus, and spleen were similar for both groups (Fig. 6A and B). At 8 dpi, an overall lower amount of rCDV^{RI}Venus(1)-L$_{H589Y}$ infection when compared to rCDV^{RI}Venus(6) infection was observed for different evaluated tissues (Fig. 6C). Importantly, this effect was even more pronounced at 20 dpi when rCDV^{RI}Venus(1)-L$_{H589Y}$-inoculated ferrets had largely cleared their infection from all lymphoid tissues, while a considerable amount of rCDV^{RI}Venus(6)-infected cells could still be detected in all tissues [N = 1 for rCDV^{RI}Venus(6)] (Fig. 6D). This finding confirms that rCDV^{RI}Venus(1)-L$_{H589Y}$-inoculated ferrets had overcome their infection.

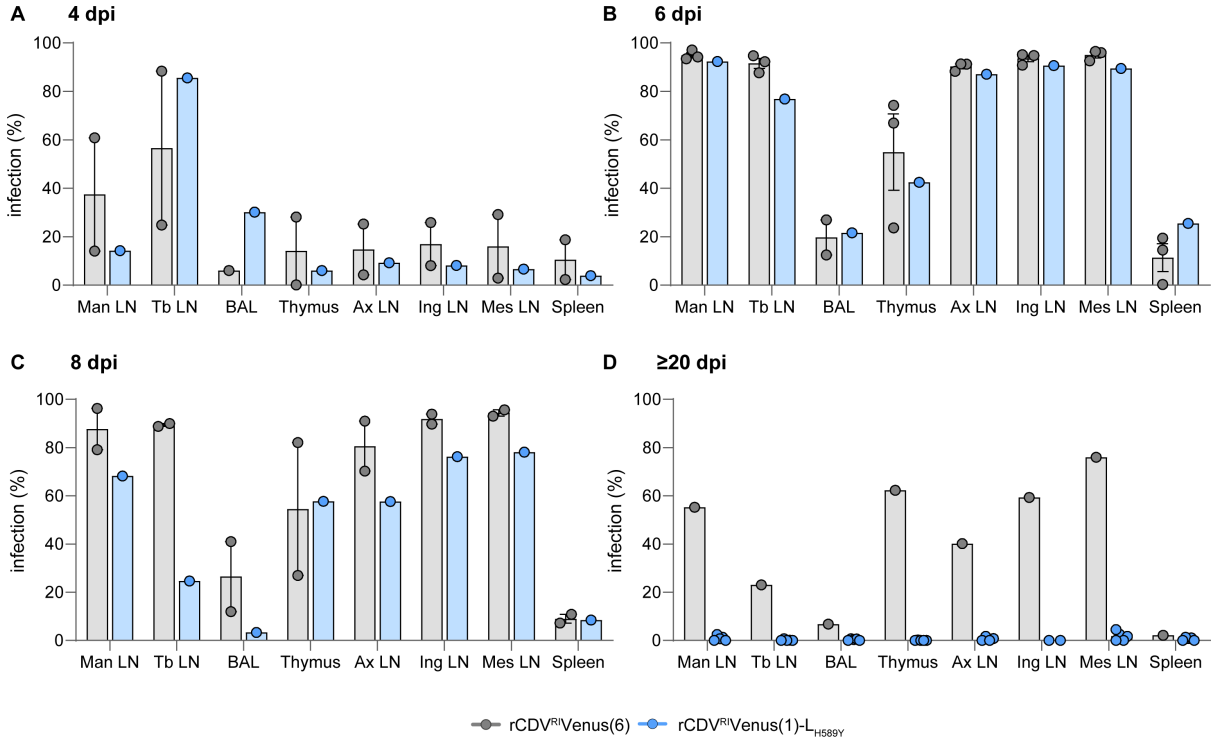

FIG 6 Detection of Venus$^+$ cells for rCDV^{RI}Venus(6)- and rCDV^{RI}Venus(1)-L$_{H589Y}$-infected animals in BAL cells and different lymphoid tissues over time. (A–D) Infection percentages were measured in single-cell suspensions from different tissues via flow cytometry at (A) 4, (B) 6, (C) 8, and (D) 20–23 dpi. The percentage of Venus$^+$ cells within the singlet gate is shown. Symbols represent individual animals, bars the average, and error bars depict the SEM. Man LN, mandibular lymph node; Tb LN, tracheobronchial lymph node; BAL, broncho-alveolar lavage; Ax LN, axillary lymph node; Ing LN, Inguinal lymph node; Mes LN, mesenteric lymph node.

DISCUSSION

We genetically modified and compared five rCDVs to rCDV^{RI}Venus(6) (33). Previously, we have reported that rCDV^{RI}Venus(6) causes severe distemper in ferrets and raccoons (18, 34). In direct comparison to rCDV^{RI}Venus(6), two rCDVs proved to be insufficiently attenuated, while rCDV^{RI}Venus(6)-L$_{EGFP}$ was too attenuated. Both polymerase point mutation rCDVs were also attenuated but were still immuno-pathogenic and were shed efficiently. rCDV^{RI}Venus(1)-L$_{H589Y}$ appeared to cause more "measles-like" disease with its lower CFR and severity score.

Other rCDV strains were previously reported to be attenuated (10, 19, 22, 25, 28, 35, 36). "Nectin-4-blind" viruses largely recapitulated the immuno-pathogenesis of measles in humans, resulting in lymphocyte infection and depletion. However, these viruses were not able to infect epithelial cells, were not transmitted, and infected animals did not show clinical manifestations (28, 35). These three aspects are crucial to fully recapitulate measles pathogenesis.

In the context of WT-based CDV, the deletion of the C protein (23, 37, 38) did not result in its attenuation. We aimed to delete the C protein by knocking out the start codon and introducing three in-frame stop codons shortly after at positions 2, 6, and 9 of the C protein. Likewise, a similar attenuation strategy of knocking out the start codon and introducing two in-frame stop codons at positions 9 and 12 also did not result in attenuation (39). However, recently it was shown that a truncated CDV-C protein can be expressed from a downstream start codon, which still maintained functionality (36). We assume that the same may have happened in our study. In our study, cloning an ATU at position 1 of the genome or an attenuating point mutation in the L gene led to lethal disease with CNS involvement in some inoculated ferrets. Previously, when EGFP was inserted at position 1 of the genome of highly pathogenic rCDV^{5804P}, n = 2/3 ferrets survived the infection, and n = 1/3 ferrets was sacrificed at the peak of disease signs (22). This difference may be related to the intrinsic virulence of the CDV strains used. Recombinant CDV^{5804P} expressing EGFP at position 6 (non-attenuated virus) infected 40% of T-cells, 57% of B-cells, and 0% of monocyte/macrophage at 7 dpi. In contrast, our comparable rCDV^{RI}Venus(6) infected approx. 90% of Th-cells, 50% of Tc-cells, similar percentages of B-cells (60%), and approx. 20% of DCs at 6 dpi, indicating an intrinsic higher virulence compared to rCDV^{5804P}.

In contrast, EGFP within the L gene highly attenuated CDV. Although inoculation of ferrets with rCDV^{RI}Venus(6)-L$_{EGFP}$ resulted in productive replication and transient lymphopenia, clinical signs were not observed. Moreover, the kinetics of replication largely differed from all other tested viruses, and only low amounts of CDV were shed. This would likely not lead to efficient transmission, an important hallmark of morbilliviruses. Previously, a similar approach was used to attenuate RPV (24). *In vitro*, the attenuated RPV strain and the parental strain grew in B95a cells at the same rate, but *in vivo* attenuation was observed, resulting in mild clinical signs and transient lymphopenia in cattle infected with the attenuated strain. Similarly, modification of CDV^{5804P} in the same way resulted in over-attenuation (25).

In this study, attenuating rCDV by introducing an ATU at position 1 (22) in combination with the point mutation H589Y in L (26) resulted in the currently best available model to mimic WT MeV. With this model, we met the majority of our pre-defined goals to accurately reflect the pathogenesis of measles: (i) rCDV^{RI}Venus(1)-L$_{H589Y}$ had an identical tropism to MeV by using CD150 and nectin-4. (ii) All rCDV^{RI}Venus(1)-L$_{H589Y}$-inoculated ferrets survived infection, showing that rCDV^{RI}Venus(1)-L$_{H589Y}$ infection is self-limiting. (iii) rCDV^{RI}Venus(1)-L$_{H589Y}$ infection resulted in transient viremia, and (iv) infected cells spread systemically to all screened lymphoid tissues. We saw similar kinetics when comparing rCDV^{RI}Venus(1)-L$_{H589Y}$ to MeV in NHP, although the peak of infection was slightly earlier (6 vs 9 dpi, respectively) (40). Infection of peripheral lymphocytes and lymphoid organs was more extensive in our CDV-ferret model than observed for MeV in NHPs. While during the peak of infection approximately 5%–10% of peripheral lymphocytes are infected by MeV, we observed almost 40% infection with

rCDV^{RI}Venus(1)-L$_{H589Y}$ (40). Similarly, infection percentages of lymphoid tissues were also higher in ferrets, but rCDV^{RI}Venus(1)-L$_{H589Y}$ was nevertheless cleared from lymphoid tissues by the end of the study. (v) As seen for MeV in NHP (40), rCDV^{RI}Venus(1)-L$_{H589Y}$ only transiently shed from the upper respiratory tract and (vi) did not result in neurological signs. (vii) rCDV^{RI}Venus(1)-L$_{H589Y}$ infection should have caused transient lymphopenia. However, in this model, lymphocyte counts did not fully recover, although systemic re-population of initially depleted myeloid cells and B-lymphocytes could be observed at 21 dpi. Previously, in a different ferret model with rCDV^{5804P} expressing EGFP at position 1, WBC counts had largely recovered by 28 dpi and fully recovered by 35 dpi, a time window that we did not explore in our study (22).

The immunosuppressive nature of rCDV^{RI}Venus(1)-L$_{H589Y}$ will allow for extension of the studies of measles-induced immune amnesia outside of the NHP model. Previously, vaccine-acquired immunity to influenza virus was shown to be compromised in ferrets after infection with nectin-4-blind CDV (10). Similarly, the effect of rCDV^{RI}Venus(1)-L$_{H589Y}$ on the immune repertoire will give insights into functional impairment, depletion, and conditions for re-population of specific memory lymphocytes. Moreover, we envision potential applications of this model for intervention studies. Although current measles vaccines are safe and effective for many, young infants and immunocompromised patients cannot be vaccinated with those live-attenuated vaccines. This model gives a platform to test new vaccine candidates. Lastly, antivirals interfering with the viral life cycle can also be tested in this model.

MATERIALS AND METHODS

Design of rCDV variants

All viruses were recombinant viruses expressing the fluorescent reporter protein Venus from an ATU. The recombinant CDVs were based on the sequence of CDV strain Rhode Island obtained from a naturally infected raccoon (33) with changes predicted to rationally attenuate the viruses. rCDV^{RI}Venus(6) and rCDV^{RI}Venus(6)-L$_{EGFP}$ have been described previously (33). rCDV^{RI}Venus(1), rCDV^{RI}Venus(6)-ΔC, rCDV^{RI}Venus(6)-L$_{H589Y}$, and rCDV^{RI}Venus(1)-L$_{H589Y}$ were recovered from plasmids pCDV^{RI}Venus(1), pCDV^{RI}Venus(6)-ΔC, pCDV^{RI}Venus(6)-L$_{H589Y}$, and pCDV^{RI}Venus(1)-L$_{H589Y}$, respectively, as previously described (33). To generate pCDV^{RI}Venus(1), pCDV^{RI} (33) was digested with Not I (in the plasmid backbone) and BbvC I (in N), and the intervening fragment was replaced (by Gibson Assembly) with a gBlock (Integrated DNA Technologies, IDT) containing a Venus-encoding transcription unit upstream of the N gene (position 1). To generate pCDV^{RI}Venus(6)-ΔC, pCDV^{RI}Venus(6) was digested with BbvC I (in N) and Sal I (downstream of the C open reading frame in P), and the intervening fragment was replaced (by Gibson Assembly) with two overlapping PCR-generated amplicons containing nucleotide mutations to knock out the start codon of the C protein and introduce three in-frame stop codons at C codon positions 2, 6, and 9 in a strategy similar to that used previously for MeV (41); the coding sequence of P is not affected by the introduced mutations. To generate pCDV^{RI}Venus(6)-L$_{H589Y}$, pCDV^{RI}Venus(6) was digested with Swa I (upstream of the modified region in L) and Xho I (downstream of the modified region in L), and the intervening fragment was replaced (by Gibson Assembly) with a gBlock (IDT) containing a nucleotide mutation to convert histidine at position 589 of the L protein to tyrosine; this mutation has been previously shown to attenuate CDV in ferrets (26). To generate pCDV^{RI}Venus(1)-L$_{H589Y}$, pCDV^{RI}Venus(1) was digested with Aat II (upstream of the modified region in L) and Xho I (downstream of the modified region in L), and the intervening fragment was replaced (by ligation) with the equivalently digested fragment from pCDV^{RI}Venus(6)-L$_{H589Y}$. An overview of viral constructs can be found in Fig. 1.

Cells

Stocks were grown on Vero-dogSLAM cells (VDS; a kind gift from Dr. Y. Yanagi) (42) or on canine lymphoblastoid cell line (CLBL) (43), and the viral load was determined by

endpoint titration on VDS. To determine receptor usage Vero cells, VDS and Vero-dog-Nectin-4 (VdN4, a kind gift from Dr. C. Richardson) cells were used. Vero, VDS, and VdN4 cells were grown in Dulbecco's modified Eagle medium, and CLBL was grown in RPMI-1640, supplemented with 10% fetal bovine serum (vol/vol), penicillin (100 IU/mL), streptomycin (100 µg/mL), and L-glutamine (2 mM).

Animal study design

Ferrets (*Mustela putorius furo*) were intratracheally inoculated with 1×10^4 $TCID_{50}$ of rCDVs. Only male ferrets were used in this study to allow for more frequent blood sampling because of their larger body size. Animals inoculated with $rCDV^{Rl}$Venus(6) were previously described, and the animals that reached their humane endpoints were used as a control group (34). The course of infection was monitored for up to 23 days post-inoculation (dpi). Throat, nose, and rectal swabs as well as WBC from whole blood and tissues were collected at various time points. We recorded the core body temperature through a temperature logger (StarOddi DST micro-T), which was implanted intra-peritoneally on average 2 weeks before the start of the study. Ferrets were euthanized at 2, 4, 6, 8, 10, 13, 14, 15, 16, 17, 20, 21, and 23 dpi by exsanguination under ketamine-medetomidine anesthesia. We retrospectively calculated the severity score of each animal and compared those to ferrets inoculated with MeV which does not replicate in ferrets and can therefore be considered negative controls (34). The severity score forms an average score of body temperature, body weight, lymphocyte counts, virus isolation from throat swabs, and infection of lymphocytes. Each parameter is classified from 0 to 3 based on severity (0 being the lowest and 3 the highest severity), and the average score of all parameters per animal is calculated (Table S1). Macroscopic fluorescence was detected using a custom-made lamp containing six 5-Volt LEDs (Luxeon Lumileds, Lambertian, cyan, peak emission 490–495 nm) mounted with D480/40 bandpass filters (Chroma), and photographs were taken using a Nikon D80 SLR camera mounted with a Dark Reader camera filter (Clare Chemical Research) (6). All numbers of animals included in different analyses are summarized in Table S2.

Flow cytometry

Frequencies of infected cells and WBC subsets in blood and tissues were determined by flow cytometry. WBCs were isolated from whole blood after red blood cell lysis with buffer (Roche). At necropsy, lymphoid tissues were collected in phosphate-buffered saline (PBS) for preparation of single-cell suspensions, processed by cutting into smaller pieces, and further dissociated with gentleMACS (Miltenyi Biotec). Single-cell suspensions from the tissues were then passed through a 100-µm filter and isolated in PBS. For WBC phenotyping, cells were stained with $CD4^{APC}$ (Clone MM02; 1:25), $CD8^{PE\text{-}Cy7}$ (Clone: OKT3; 1:25), $CD11b^{AmCyan}$ (Clone: M1/70, 1:25), and $HLA\text{-}DR^{APC\text{-}Cy7}$ (Clone: L243; 1:25) antibodies; on average, more than 4×10^5 events were recorded. Subsets were defined using FSC and SSC as well as the cell-surface markers. Th-lymphocytes were defined as FSC^{low}, $CD11b^-$, $HLA\text{-}DR^-$, $CD4^+$; Tc-lymphocytes were defined as FSC^{low}, $CD11b^-$, $HLA\text{-}DR^-$, $CD8^+$; B-lymphocytes were defined as FSC^{low}, $CD11b^-$, $HLA\text{-}DR^+$; DCs were defined as FSC^{high}, $CD11b^{high}$, $HLA\text{-}DR^{high}$; monocytes were defined as FSC^{low}, $CD11b^{high}$, $HLA\text{-}DR^{inter}$; granulocytes were defined as FSC^{low}, $CD11b^{high}$, $HLA\text{-}DR^-$. The percentage of infected cells was determined by detection of $Venus^+$ cells in each subset. All data were analyzed using FlowJo software. A gating strategy can be found in Fig. S3.

Virus isolation

Throat, nose, and rectal swabs were resuspended in a 2-mL virus transport medium (VTM). Upon one freeze-thaw cycle, virus-containing VTM was titrated on VDS in a threefold dilution series. For virus isolation from WBC, 80,000 WBCs were diluted in 1 mL, and then a twofold dilution series was performed on VDS. Four days post virus isolation,

viral load was determined by fluorescence detection, and virus titer ($TCID_{50}$/mL) was calculated using the Reed-Muench method (44).

ACKNOWLEDGMENTS

The authors thank Lennert Gommers and Laurine C. Rijsbergen for technical support and the employees of the animal facility of Erasmus MC for their help.

This work was in part funded by the Defense Advanced Research Projects Agency (DARPA) INTERfering and Co-Evolving Prevention and Therapy (INTERCEPT) program (grant HR0011940493), Boston University.

AUTHOR AFFILIATIONS

[1]Department of Viroscience, Erasmus MC, Rotterdam, the Netherlands
[2]Center for Vaccine Research, University of Pittsburgh School of Medicine, Pittsburgh, Pennsylvania, USA

AUTHOR ORCIDs

Katharina S. Schmitz http://orcid.org/0000-0002-8537-0646
Linda J. Rennick http://orcid.org/0000-0001-5974-6921
Natasha L. Tilston-Lunel http://orcid.org/0000-0002-5290-9350
Rik L. de Swart http://orcid.org/0000-0003-3599-8969
W. Paul Duprex http://orcid.org/0000-0003-1716-6376

FUNDING

Funder	Grant(s)	Author(s)
DOD | Defense Advanced Research Projects Agency (DARPA)	HR0011940493	W. Paul Duprex

AUTHOR CONTRIBUTIONS

Katharina S. Schmitz, Investigation, Methodology, Project administration, Visualization, Writing – original draft, Writing – review and editing | Linda J. Rennick, Investigation, Methodology, Writing – review and editing | Natasha L. Tilston-Lunel, Investigation, Methodology, Writing – review and editing | Anouskha D. Comvalius, Investigation, Methodology | Brigitta M. Laksono, Investigation, Methodology, Writing – review and editing | Daryl Geers, Investigation, Writing – review and editing | Peter van Run, Investigation, Methodology | Rory D. de Vries, Conceptualization, Supervision, Visualization, Writing – review and editing | Rik L. de Swart, Conceptualization, Funding acquisition, Investigation, Methodology, Resources, Writing – review and editing | W. Paul Duprex, Conceptualization, Funding acquisition, Supervision, Writing – review and editing

ETHICS APPROVAL

Male ferrets (0.8–1.5 kg) were obtained from a commercial vendor. Animals were housed, and experiments were performed in compliance with the Dutch legislation for the protection of animals used for scientific purposes (Animals Experiments Act 2014, implementing EU Directive 2010/63). Research was conducted under a project license from the Dutch competent authority, ethically reviewed by the Animal Experiments Committee, and the study protocol was approved by the Institutional Animal Welfare Body. Animal welfare was monitored on a daily basis. Ferrets were housed in groups prior to inoculation, received species-specific food on a daily basis, and had access to water *ad libitum*. Cages contained several sources of environmental enrichment. Acclimatization period was at least 3 weeks. During the infection studies, ferrets were randomly assigned to a group and housed in groups of three in HEPA-filtered, negatively

pressurized biosafety level 3 isolators. Animal handling was performed under anesthesia using ketamine and medetomidine. After handling, atipamezole was administered to antagonize the effect of medetomidine. The researchers were not blinded during the analyses. Humane endpoints were pre-defined as (i) animals stop eating and drinking, (ii) loss of >20% body weight, (iii) severe respiratory distress, (iv) abnormal movement and / or behavior suggestive of CNS invasion, and (v) severe wounds as a result of social interactions. This manuscript was prepared in accordance with the ARRIVE guidelines (45).

ADDITIONAL FILES

The following material is available online.

Supplemental Material

Supplemental material (JVI01850-23-s0001.pdf). Tables S1 and S2; Figures S1 to S3.

REFERENCES

1. Rima B, Balkema-Buschmann A, Dundon WG, Duprex P, Easton A, Fouchier R, Kurath G, Lamb R, Lee B, Rota P, Wang L, ICTV Report Consortium. 2019. ICTV virus taxonomy profile: *Paramyxoviridae*. J Gen Virol 100:1593–1594. https://doi.org/10.1099/jgv.0.001328
2. Minta AA, Ferrari M, Antoni S, Portnoy A, Sbarra A, Lambert B, Hauryski S, Hatcher C, Nedelec Y, Datta D, Ho LL, Steulet C, Gacic-Dobo M, Rota PA, Mulders MN, Bose AS, Perea WA, O'Connor P. 2022. Progress toward regional measles elimination — worldwide, 2000–2021. MMWR Morb Mortal Wkly Rep 71:1489–1495. https://doi.org/10.15585/mmwr.mm7147a1
3. Tatsuo H, Ono N, Tanaka K, Yanagi Y. 2000. SLAM (CDw150) is a cellular receptor for measles virus. Nature 406:893–897. https://doi.org/10.1038/35022579
4. Lemon K, de Vries RD, Mesman AW, McQuaid S, van Amerongen G, Yüksel S, Ludlow M, Rennick LJ, Kuiken T, Rima BK, Geijtenbeek TBH, Osterhaus ADME, Duprex WP, de Swart RL. 2011. Early target cells of measles virus after aerosol infection of non-human primates. PLoS Pathog 7:e1001263. https://doi.org/10.1371/journal.ppat.1001263
5. de Vries RD, de Swart RL. 2014. Measles immune suppression: functional impairment or numbers game? PLoS Pathog 10:e1004482. https://doi.org/10.1371/journal.ppat.1004482
6. de Vries RD, McQuaid S, van Amerongen G, Yüksel S, Verburgh RJ, Osterhaus ADME, Duprex WP, de Swart RL. 2012. Measles immune suppression: lessons from the macaque model. PLoS Pathog 8:e1002885. https://doi.org/10.1371/journal.ppat.1002885
7. Mina MJ, Metcalf CJE, de Swart RL, Osterhaus ADME, Grenfell BT. 2015. Long-term measles-induced immunomodulation increases overall childhood infectious disease mortality. Science 348:694–699. https://doi.org/10.1126/science.aaa3662
8. Laksono BM, de Vries RD, Verburgh RJ, Visser EG, de Jong A, Fraaij PLA, Ruijs WLM, Nieuwenhuijse DF, van den Ham H-J, Koopmans MPG, van Zelm MC, Osterhaus ADME, de Swart RL. 2018. Studies into the mechanism of measles-associated immune suppression during a measles outbreak in the Netherlands. Nat Commun 9:4944. https://doi.org/10.1038/s41467-018-07515-0
9. Mina MJ, Kula T, Leng Y, Li M, de Vries RD, Knip M, Siljander H, Rewers M, Choy DF, Wilson MS, Larman HB, Nelson AN, Griffin DE, de Swart RL, Elledge SJ. 2019. Measles virus infection diminishes preexisting antibodies that offer protection from other pathogens. Science 366:599–606. https://doi.org/10.1126/science.aay6485
10. Petrova VN, Sawatsky B, Han AX, Laksono BM, Walz L, Parker E, Pieper K, Anderson CA, de Vries RD, Lanzavecchia A, Kellam P, von Messling V, de Swart RL, Russell CA. 2019. Incomplete genetic reconstitution of B cell pools contributes to prolonged immunosuppression after measles. Sci Immunol 4:eaay6125. https://doi.org/10.1126/sciimmunol.aay6125
11. Mühlebach MD, Mateo M, Sinn PL, Prüfer S, Uhlig KM, Leonard VHJ, Navaratnarajah CK, Frenzke M, Wong XX, Sawatsky B, Ramachandran S, McCray PB, Cichutek K, von Messling V, Lopez M, Cattaneo R. 2011. Adherens junction protein nectin-4 is the epithelial receptor for measles virus. Nature 480:530–533. https://doi.org/10.1038/nature10639
12. Noyce RS, Bondre DG, Ha MN, Lin LT, Sisson G, Tsao MS, Richardson CD. 2011. Tumor cell marker PVRL4 (nectin 4) is an epithelial cell receptor for measles virus. PLoS Pathog 7:e1002240. https://doi.org/10.1371/journal.ppat.1002240
13. Racaniello V. 2011. An exit strategy for measles virus. Science 334:1650–1651. https://doi.org/10.1126/science.1217378
14. de Swart RL. 2009. Measles studies in the macaque model. Curr Top Microbiol Immunol 330:55–72. https://doi.org/10.1007/978-3-540-70617-5_3
15. Sellin CI, Davoust N, Guillaume V, Baas D, Belin MF, Buckland R, Wild TF, Horvat B. 2006. High pathogenicity of wild-type measles virus infection in CD150 (SLAM) transgenic mice. J Virol 80:6420–6429. https://doi.org/10.1128/JVI.00209-06
16. Ferreira CSA, Frenzke M, Leonard VHJ, Welstead GG, Richardson CD, Cattaneo R. 2010. Measles virus infection of alveolar macrophages and dendritic cells precedes spread to lymphatic organs in transgenic mice expressing human signaling lymphocytic activation molecule. J Virol 84:3033–3042. https://doi.org/10.1128/JVI.01559-09
17. Nambulli S, Sharp CR, Acciardo AS, Drexler JF, Duprex WP. 2016. Mapping the evolutionary trajectories of morbilliviruses: what, where and whither. Curr Opin Virol 16:95–105. https://doi.org/10.1016/j.coviro.2016.01.019
18. Roelofs D, Schmitz KS, van Amerongen G, Rijsbergen LC, Laksono BM, Comvalius AD, Nambulli S, Rennick LJ, van Run P, Duprex WP, van den Brand JMA, de Swart RL, de Vries RD. 2023. Inoculation of raccoons with a wild-type-based recombinant canine distemper virus results in viremia, lymphopenia, fever, and widespread histological lesions. mSphere 8:e0014423. https://doi.org/10.1128/msphere.00144-23
19. von Messling V, Springfeld C, Devaux P, Cattaneo R. 2003. A ferret model of canine distemper virus virulence and immunosuppression. J Virol 77:12579–12591. https://doi.org/10.1128/JVI.77.23.12579-12591.2003
20. da Fontoura Budaszewski R, von Messling V. 2016. Morbillivirus experimental animal models: measles virus pathogenesis insights from canine distemper virus. Viruses 8:274. https://doi.org/10.3390/v8100274
21. Cattaneo R, Rebmann G, Schmid A, Baczko K, ter Meulen V, Billeter MA. 1987. Altered transcription of a defective measles virus genome derived from a diseased human brain. EMBO J 6:681–688. https://doi.org/10.1002/j.1460-2075.1987.tb04808.x
22. von Messling V, Milosevic D, Cattaneo R. 2004. Tropism illuminated: lymphocyte-based pathways blazed by lethal morbillivirus through the host immune system. Proc Natl Acad Sci U S A 101:14216–14221. https://doi.org/10.1073/pnas.0403597101
23. Devaux P, Hodge G, McChesney MB, Cattaneo R. 2008. Attenuation of V- or C-defective measles viruses: infection control by the inflammatory and interferon responses of rhesus monkeys. J Virol 82:5359–5367. https://doi.org/10.1128/JVI.00169-08

24. Brown DD, Rima BK, Allen IV, Baron MD, Banyard AC, Barrett T, Duprex WP. 2005. Rational attenuation of a morbillivirus by modulating the activity of the RNA-dependent RNA polymerase. J Virol 79:14330–14338. https://doi.org/10.1128/JVI.79.22.14330-14338.2005
25. Silin D, Lyubomska O, Ludlow M, Duprex WP, Rima BK. 2007. Development of a challenge-protective vaccine concept by modification of the viral RNA-dependent RNA polymerase of canine distemper virus. J Virol 81:13649–13658. https://doi.org/10.1128/JVI.01385-07
26. Krumm SA, Yan D, Hovingh ES, Evers TJ, Enkirch T, Reddy GP, Sun A, Saindane MT, Arrendale RF, Painter G, Liotta DC, Natchus MG, von Messling V, Plemper RK. 2014. An orally available, small-molecule polymerase inhibitor shows efficacy against a lethal morbillivirus infection in a large animal model. Sci Transl Med 6:232ra52. https://doi.org/10.1126/scitranslmed.3008517
27. Leonard VHJ, Hodge G, Reyes-Del Valle J, McChesney MB, Cattaneo R. 2010. Measles virus selectively blind to signaling lymphocytic activation molecule (SLAM; CD150) is attenuated and induces strong adaptive immune responses in rhesus monkeys. J Virol 84:3413–3420. https://doi.org/10.1128/JVI.02304-09
28. Sawatsky B, Wong X-X, Hinkelmann S, Cattaneo R, von Messling V. 2012. Canine distemper virus epithelial cell infection is required for clinical disease but not for immunosuppression. J Virol 86:3658–3666. https://doi.org/10.1128/JVI.06414-11
29. Laksono BM, de Vries RD, Duprex WP, de Swart RL. 2020. Measles pathogenesis, immune suppression and animal models. Curr Opin Virol 41:31–37. https://doi.org/10.1016/j.coviro.2020.03.002
30. Leonard VHJ, Sinn PL, Hodge G, Miest T, Devaux P, Oezguen N, Braun W, McCray PB Jr, McChesney MB, Cattaneo R. 2008. Measles virus blind to its epithelial cell receptor remains virulent in rhesus monkeys but cannot cross the airway epithelium and is not shed. J Clin Invest 118:2448–2458. https://doi.org/10.1172/JCI35454
31. Rota PA, Moss WJ, Takeda M, de Swart RL, Thompson KM, Goodson JL. 2016. Measles. Nat Rev Dis Primers 2:16049. https://doi.org/10.1038/nrdp.2016.49
32. Delpeut S, Sawatsky B, Wong X-X, Frenzke M, Cattaneo R, von Messling V. 2017. Nectin-4 interactions govern measles virus virulence in a new model of pathogenesis, the squirrel monkey (*Saimiri sciureus*). J Virol 91:e02490-16. https://doi.org/10.1128/JVI.02490-16
33. Tilston-Lunel NL, Welch SR, Nambulli S, de Vries RD, Ho GW, Wentworth DE, Shabman R, Nichol ST, Spiropoulou CF, de Swart RL, Rennick LJ, Duprex WP. 2021. Sustained replication of synthetic canine distemper virus defective genomes *in vitro* and *in vivo*. mSphere 6. https://doi.org/10.1128/mSphere.00537-21
34. Laksono BM, Roelofs D, Comvalius AD, Schmitz KS, Rijsbergen LC, Geers D, Nambulli S, van Run P, Duprex WP, van den Brand JMA, de Vries RD, de Swart RL. 2023. Infection of ferrets with wild type-based recombinant canine distemper virus overwhelms the immune system and causes fatal systemic disease. mSphere 8:e0008223. https://doi.org/10.1128/msphere.00082-23
35. Sawatsky B, Cattaneo R, von Messling V. 2018. Canine distemper virus spread and transmission to naive ferrets: selective pressure on signaling lymphocyte activation molecule-dependent entry. J Virol 92:e00669-18. https://doi.org/10.1128/JVI.00669-18
36. Siering O, Sawatsky B, Pfaller CK. 2021. C protein is essential for canine distemper virus virulence and pathogenicity in ferrets. J Virol 95:e01840-20. https://doi.org/10.1128/JVI.01840-20
37. Toth AM, Devaux P, Cattaneo R, Samuel CE. 2009. Protein kinase PKR mediates the apoptosis induction and growth restriction phenotypes of C protein-deficient measles virus. J Virol 83:961–968. https://doi.org/10.1128/JVI.01669-08
38. McAllister CS, Toth AM, Zhang P, Devaux P, Cattaneo R, Samuel CE. 2010. Mechanisms of protein kinase PKR-mediated amplification of beta interferon induction by C protein-deficient measles virus. J Virol 84:380–386. https://doi.org/10.1128/JVI.02630-08
39. von Messling V, Svitek N, Cattaneo R. 2006. Receptor (SLAM [CD150]) recognition and the V protein sustain swift lymphocyte-based invasion of mucosal tissue and lymphatic organs by a morbillivirus. J Virol 80:6084–6092. https://doi.org/10.1128/JVI.00357-06
40. de Swart RL, Ludlow M, de Witte L, Yanagi Y, van Amerongen G, McQuaid S, Yüksel S, Geijtenbeek TBH, Duprex WP, Osterhaus ADME. 2007. Predominant infection of CD150$^+$ lymphocytes and dendritic cells during measles virus infection of macaques. PLoS Pathog 3:e178. https://doi.org/10.1371/journal.ppat.0030178
41. Radecke F, Billeter MA. 1996. The nonstructural C protein is not essential for multiplication of Edmonston B strain measles virus in cultured cells. Virology 217:418–421. https://doi.org/10.1006/viro.1996.0134
42. Seki F, Ono N, Yamaguchi R, Yanagi Y. 2003. Efficient isolation of wild strains of canine distemper virus in vero cells expressing canine SLAM (CD150) and their adaptability to marmoset B95a cells. J Virol 77:9943–9950. https://doi.org/10.1128/JVI.77.18.9943-9950.2003
43. Rütgen BC, Hammer SE, Gerner W, Christian M, de Arespacochaga AG, Willmann M, Kleiter M, Schwendenwein I, Saalmüller A. 2010. Establishment and characterization of a novel canine B-cell line derived from a spontaneously occurring diffuse large cell lymphoma. Leuk Res 34:932–938. https://doi.org/10.1016/j.leukres.2010.01.021
44. Reed LJ, Muench H. 1938. A simple method of estimating fifty per cent endpoints. Am J Epidemiol 27:493–497. https://doi.org/10.1093/oxfordjournals.aje.a118408
45. Percie du Sert N, Hurst V, Ahluwalia A, Alam S, Avey MT, Baker M, Browne WJ, Clark A, Cuthill IC, Dirnagl U, et al. 2020. The ARRIVE guidelines 2.0: updated guidelines for reporting animal research. PLoS Biol 18:e3000410. https://doi.org/10.1371/journal.pbio.3000410